JOURNAL OF CHEMICAL PHYSICS VOLUME 117, NUMBER 4 22 JULY 2002

# A theoretical study of ozone isotopic effects using a modified *ab initio* potential energy surface

Yi Qin Gao, Wei-Chen Chen, and R. A. Marcus<sup>a)</sup>
Noyes Laboratories, California Institute of Technology, Pasadena, California 91125

(Received 12 February 2002; accepted 3 May 2002)

A modified *ab initio* potential energy surface (PES) is used for calculations of ozone recombination and isotopic exchange rate constants. The calculated low-pressure isotopic effects on the ozone formation reaction are consistent with the experimental results and with the theoretical results obtained earlier [J. Chem. Phys. **116**, 137 (2002)]. They are thereby relatively insensitive to the properties of these PES. The topics discussed include the dependence of the calculated low-pressure recombination rate constant on the hindered-rotor PES, the role of the asymmetry of the potential for a general X+YZ reaction ( $Y \neq Z$ ), and the partitioning to form each of the two recombination products: XYZ and XZY. © 2002 American Institute of Physics. [DOI: 10.1063/1.1488577]

#### I. INTRODUCTION

We have treated the unusual isotopic effects<sup>1–28</sup> of ozone formation earlier using both loose and hindered-rotor transition states.<sup>29,30</sup> Because of the lack of an accurate potential energy surface (PES) in the vicinity of the hindered-rotor transition state, a model PES was used for recombination and isotopic exchange reactions.<sup>29,30</sup> This model PES was chosen to fit the experimentally<sup>31</sup> obtained negative temperature dependence of the ozone isotopic exchange rate constant. In the present study a modified<sup>32</sup> *ab initio* PES is used instead and the effect on the calculated rate constant ratios of the many isotopic systems is discussed.

In addition to using a modified *ab initio* PES, a new and more sophisticated way is given for weighting the relative yields of the reaction products XYZ and XZY in the recombination of X and YZ. The method can also be used for more general PES. For simplicity, this weighting factor was assumed earlier<sup>29,30</sup> to be 1/2 for each product. The more general weighting in the present study is obtained by an integration of the squared magnitude of each wave function over the angular space that leads to the desired product. These two methods are then compared in the treatment of ozone isotopic exchange and recombination reactions.

The microscopic rate constants themselves are calculated using a modified RRKM theory with the transition state for each quantum state determined variationally, as before. <sup>29,30</sup> An  $\eta$  effect, which reduces the low-pressure rate constant for the formation of a symmetric molecule more than that for an asymmetric one, is also included. <sup>29,30</sup> The  $\eta$  effect is a small correction ( $\sim$ 15%) and its origin has been described previously. <sup>29,33,34</sup> This correction is apart from symmetry numbers, which are also included.

For the deactivation of the vibrationally excited ozone molecules a master equation formalism is used. It was obtained earlier<sup>30</sup> using a weak collision model. In this weak collisional energy transfer model, the energy transfer is as-

sumed to be stepwise, and a strong collisional angular momentum transfer assumption is used. 30,35 In the low-pressure limit the vibrationally excited ozone molecules with energies above the dissociation threshold can only experience at most a single collision with the bath molecules before redissociation. As a result in a weak collision model only low energy states can be stabilized significantly at low pressures and form stable ozone molecules. 29,30

One difference between the two exit channels X+YZand XY + Z for the dissociation of any asymmetric molecule XYZ  $(X \neq Z)$  is the difference between the zero-point energies of YZ and YX. At any given energy, this difference of zero-point energies favors the reaction through the channel with the smaller zero-point energy because of the greater number of quantum states in the transition state for that exit channel. This difference between the respective number of quantum states of the transition states for the two exit channels is large at low energies.<sup>30</sup> Since weak collisions sample mainly low energy states, a large difference occurs between the rate constants via the two recombination channels leading to an XYZ at low pressures. 30 Since the zero-point energy difference between YZ and YX depends mainly on the mass difference between Z and X, this weak collision effect leads to a strikingly large mass dependence of individual rate constant ratios when reaction occurs only via one of the two channels ("unscrambled systems"). 24-28 In particular, in unscrambled experiments vibrationally excited ozone isotopomers  $XYY^*$  are formed only from  $X+YY\rightarrow XYY^*$  and not from  $Y + YX \rightarrow XYY^*$ .

In a scrambled system both such channels are allowed since extensive isotopic exchange occurs via  $XYZ^*$  between X+YZ and Z+YX. As a result, it was shown that the partitioning effect between the two exit channels disappears exactly.<sup>33</sup> Instead, one observes the difference between the formation rates of symmetric and asymmetric molecules and the resulting mass-independent effect ("symmetry driven") arises.<sup>29,30,33,34</sup>

The present study was performed to test further the numerical aspects of the theory using a more elaborate ozone

a) Author to whom correspondence should be addressed. Electronic mail: ram@caltech.edu

PES. We suggested in an earlier paper<sup>30</sup> that the low-pressure results on enrichments and rate constant ratios would be relatively insensitive to the hindered-rotor potential energy surface used. The present study provides a test of this suggestion. The ozone recombination rate constant ratios and the enrichments for different isotopomers are calculated, together with the rate constant of the ozone isotopic exchange reaction  $^{16}\text{O} + ^{18}\text{O}^{18}\text{O} \rightarrow ^{18}\text{O} + ^{16}\text{O}^{18}\text{O}$  and its temperature dependence. They are compared with the experimental data and with the previous theoretical results.

The paper is organized as follows: The PES used is summarized in Sec. II. The hindered rotor eigenstates are obtained in Sec. III, and are used to calculate rate constants in Sec. IV. The results are discussed in Sec. V.

#### **II. POTENTIAL ENERGY SURFACE**

The underlying *ab initio* ozone PES is that of Morokuma and co-workers, <sup>36</sup> who used the MOLPRO program within the range of  $95^{\circ} \le \alpha \le 135^{\circ}$ ,  $2.1a_0 \le r_1 \le 3.0a_0$ , and  $2.1a_0 \le r_2 \le 5.0a_0$ , where  $\alpha$  is the bond angle and  $r_1$  and  $r_2$  are the bond lengths. This PES was fitted by the same authors to a Murrell–Sorbie analytical function. To be consistent with the experimentally determined negative temperature dependence of the recombination rate constant, <sup>37</sup> an exponential term was added to the Murrell–Sorbie analytical function by Cross and Billing <sup>32</sup> in their molecular dynamic studies of the ozone recombination reaction. It removed a local  $\sim 0.15$  eV maximum in the energy barrier for recombination on the original *ab initio* PES. This modified PES is the one used in the present study.

The reaction coordinate is again taken, for simplicity, as the distance R between the oxygen atom and the center of mass of the oxygen molecule fragment. The modified ab initio potential energy surface is written as  $V_0(R) + V(R,\theta)$ , where  $V_0(R)$  is taken as the minimum of the potential energy at R, minimized with respect to  $\theta$ , and  $V(R,\theta)$  is the angular dependence of the PES at the given R;  $\theta$  is the angle between the oxygen molecular bond and the line connecting the center of mass of this oxygen molecule and the oxygen atom. The  $V(R,\theta)$  is fitted to

$$V(R,\theta) = \sum_{i=0}^{d} b_i(R)\cos^i\theta,$$
 (1)

where d is the highest order of the expansion. Only for a homonuclear fragment YY do all the odd terms in Eq. (1) vanish. The  $V_0$  is given as a function of R in Fig. 1, and  $V(R,\theta)$  and a fitting function are depicted for different values of R in Fig. 2. A contour plot of the PES is given as a function of R and  $\theta$  in Fig. 3.

## III. THE HINDERED-ROTOR EIGENSTATES

The orbital and hindered-rotational components of the Hamiltonian for the transition state region for a three body system  $X \cdots YZ$  is written as

$$H = \frac{\hbar^2}{2\mu R^2} \mathbf{l}^2 + \frac{\hbar^2}{2I} \mathbf{j}^2 + V(R, \theta, \phi),$$
 (2)

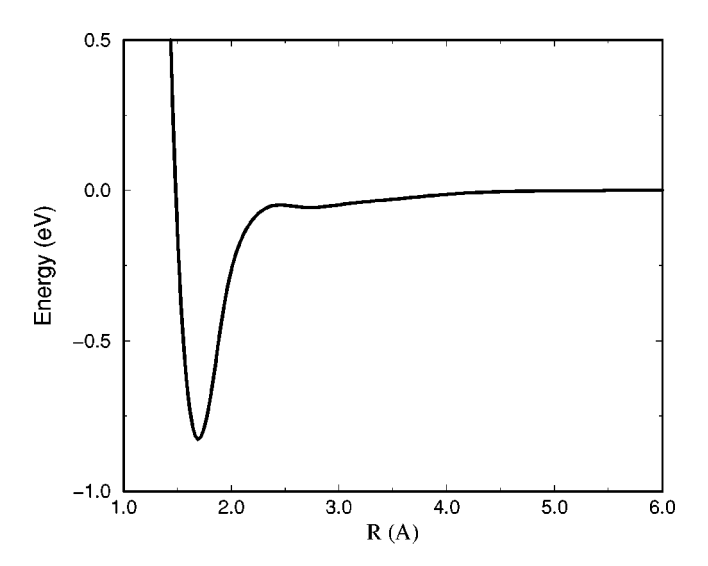


FIG. 1.  $V_0$  as a function of R.

where  $\mu$  is the reduced mass of  $X \cdots YZ$ , R is the distance between X and the center of mass of YZ, I the moment of inertia of YZ,  $I\hbar$  the orbital angular momentum operator, and  $j\hbar$  the angular momentum operator for the rotation of the fragment YZ

$$\mathbf{j}^2 = -\frac{1}{\sin\theta} \frac{\partial}{\partial\theta} \left( \sin\theta \frac{\partial}{\partial\theta} \right) + \frac{m^2}{\sin^2\theta}.$$
 (3)

In Eq. (3) m is the projection of  $\mathbf{j}$  onto the axis connecting the X and the center of mass of YZ. The total angular momentum operator  $\mathbf{J}$  is then

$$\mathbf{J} = \mathbf{j} + \mathbf{l},\tag{4}$$

the projection of which along the line connecting the centers of mass is also m.

Combining Eqs. (2) and (4) and neglecting terms off diagonal in m, as discussed in Refs. 30 and 38, one obtains

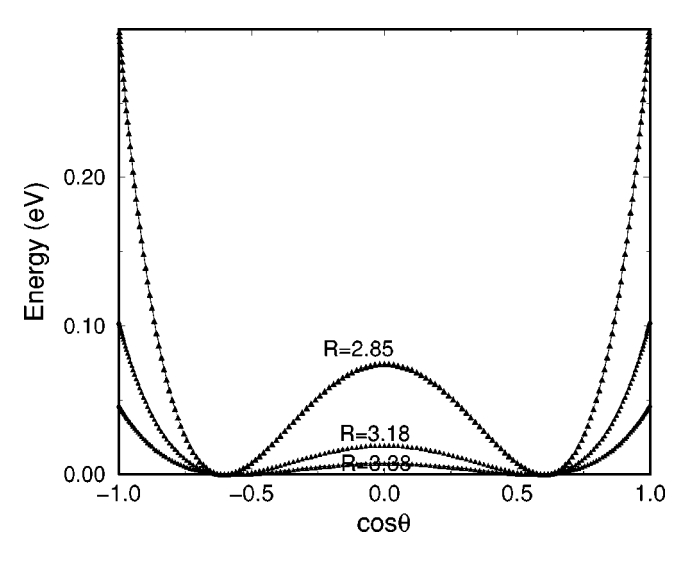


FIG. 2.  $V(R, \theta)$  vs cos  $\theta$  for a symmetric fragment YY + X, where X may or may not be the same as Y, for different values of R (in units of Å).

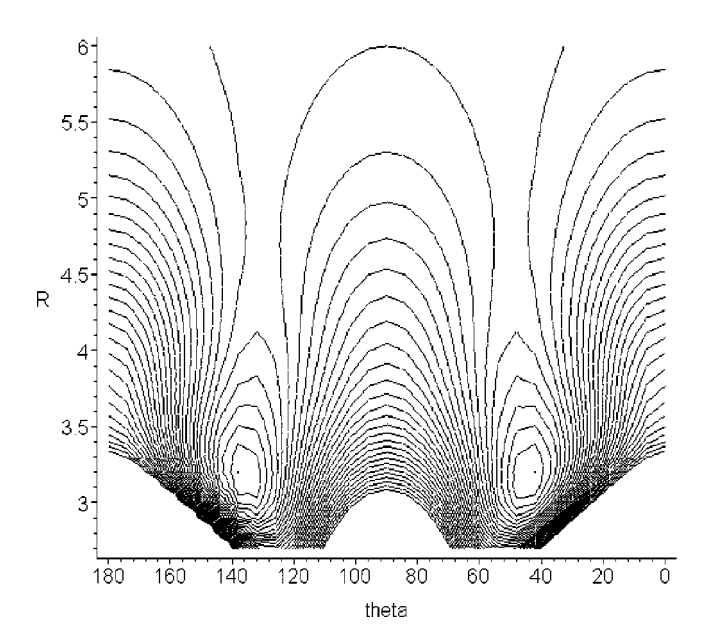


FIG. 3. Contour plot of the potential energy surface as a function of R and  $\theta$  for  $^{16}{\rm O}+^{16}{\rm O}^{16}{\rm O}$ .

$$H = \frac{\hbar^2}{2\mu R^2} \mathbf{J}^2 - \frac{\hbar^2}{\mu R^2} m^2 + \left(\frac{\hbar^2}{2\mu R^2} + \frac{\hbar^2}{2I}\right) \mathbf{j}^2 + V(R, \theta). \tag{5}$$

(In Appendix A of Ref. 30 m is denoted by  $\Omega$ .) The first two terms on the right-hand side of Eq. (5) are constants for given J and m. To obtain the eigenvalues of H we focus first on the third and fourth terms on the right-hand side of Eq. (5). Using Eq. (3) these two terms can be written as

$$H_{1} = -\left(\frac{\hbar^{2}}{2I} + \frac{\hbar^{2}}{2\mu R^{2}}\right) \frac{d}{d\zeta} \left[ (1 - \zeta^{2}) \frac{d}{d\zeta} \right] + \left(\frac{\hbar^{2}}{2I} + \frac{\hbar^{2}}{2\mu R^{2}}\right) \frac{m^{2}}{1 - \zeta^{2}} + V_{R}(\zeta), \tag{6}$$

where  $\zeta = \cos \theta$  and  $V_R(\zeta)$  denotes  $V(R,\theta)$ . The angle when Z in ZY is the closer one to X lies in the interval  $(0,\pi/2)$  while when Y is closer to X,  $\theta$  lies in the interval  $(\pi/2,\pi)$ .

The solution  $\Psi_{mj}$  of  $H_1\Psi_{mj} = E_{mj}\Psi_{mj}$  can be written as a linear combination of associated Legendre polynomials  $P_n^m$  for the given m

$$\Psi_{mj}(\zeta) = \sum_{k=0}^{\infty} d_k^{mj} P_{m+k}^m(\zeta). \tag{7}$$

Substitution of Eq. (7) into Eq. (6) and using 40

$$-\frac{d}{d\zeta} \left[ (1-\zeta)^2 \frac{d}{d\zeta} P_n^m \right] + \frac{m^2}{1-\zeta^2} P_n^m = n(n+1) P_n^m,$$
 (8)

one obtains

$$\left(\frac{\hbar^2}{2I} + \frac{\hbar^2}{2\mu R^2}\right) \sum_{k=0}^{\infty} d_k^{mj} [(m+k)(m+k+1) - E_{mj}]$$

$$\times P_{m+k}^{m}(\zeta) + \sum_{k=0}^{\infty} d_{k}^{mj} V_{R}(\zeta) P_{m+k}^{m}(\zeta) = 0.$$
 (9)

Using the recurrence relation<sup>40</sup>

$$(2n+1)\zeta P_n^m(\zeta) = (n+m)P_{n-1}^m(\zeta) + (n-m+1)P_{n+1}^m(\zeta),$$
(10)

and the expansion  $V_R(\zeta) = \sum_{i=0}^d b_i \zeta^i$  the term  $V_R(\zeta) P_{m+k}^m(\zeta)$  can be written as a sum of associated Legendre polynomials

$$V_{R}(\zeta)P_{m+k}^{m}(\zeta) = \sum_{i=-d}^{d} \alpha_{i}P_{m+k+i}^{m}(\zeta).$$
 (11)

Combining Eqs. (9) and (11) and noting the independence of the  $P_{m+k}^m$ s one obtains a set of linear equations for the coefficients  $d_k^{mj}$  in Eq. (9)

$$\alpha_{-d}d_{k-d}^{mj} + \dots + \alpha_{-1}d_{k-1}^{mj} + d_k^{mj} \times [(m+k)(m+k+1) - E_{mj}] + \alpha_1 d_{k+1}^{mj} + \dots + \alpha_d d_{k+d}^{mj} = 0.$$
(12)

The eigenvalues and the eigenvectors are obtained from Eq. (12). The wave functions of the hindered-rotor states with the quantum number m and all  $j \ge m$  are then obtained using Eq. (7).

## IV. RATE CONSTANTS AND ENRICHMENTS

The rate constant for an exchange reaction, such as

$$^{16}O + ^{18}O^{18}O \rightarrow ^{18}O + ^{16}O^{18}O$$
 (13)

can be written as<sup>34</sup>

$$k_{\text{ex}}^{a} = \frac{1}{hQ_{a}} \sum_{J} \int_{E} \frac{N_{a}(EJ)N_{b}(EJ)}{N_{a}(EJ) + N_{b}(EJ)} e^{-E/k_{B}T} dE,$$
 (14)

where  $Q_a$  is the partition function of the reacting pair in the center of the mass system of coordinates for channel a, and  $N_{a(b)}(EJ)$  is the number of states of the transition state for exit channel a(b) of ozone dissociation at the given E and J. The a denotes the exit channel with the smaller zero-point energy. In the case of the reaction in Eq. (13) it is  $^{16}\text{O} + ^{18}\text{O}^{18}\text{O}$ . Each of the two exit channels has its own transition state, determined variationally, as discussed later.

Since the reactants X+YZ ( $Y\neq Z$ ) can lead to two different recombination products, XYZ and XZY, and the phase space for the transition state can be divided into two subspaces, each leading to a different ozone product. A weighting factor  $\Phi_{a(b)}$  ( $\Phi_a+\Phi_b=1$ ) for each quantum state is assigned to each product. The  $\Phi_{a(b)}$  is taken as the squared amplitude of the normalized wave functions  $\Psi_{mj}(\zeta)$ , integrated over half of the  $\theta$  space, the half that corresponds to the desired product XYZ

$$\Phi_a(mj) = \int_{\zeta=0}^1 |\Psi_{mj}(\zeta)|^2 d\zeta. \tag{15}$$

In the other half of the  $\theta$  space  $\zeta$  lies in the interval (-1,0). <sup>39</sup>

When an asymmetric ozone molecule XYZ is formed, it is helpful to distinguish between two different weighting factors: The  $\Phi_a$  defined in Eq. (15) arises from the fact that when  $Y \neq Z$  there exists a competing channel in which the same reactants, X+YZ, lead to XZY instead of XYZ. We define a "global" transition state  $X\cdots YZ$  as one for the entire  $\theta$  interval  $(0, \pi)$  in which part of this  $\theta$  interval leads to XYZ and the other part to XZY (cf Fig. 5). On the other hand, for the formation of any product XYZ there also exist two competing entrance channels, one from X+YZ and the other from XY+Z when  $X\neq Z$ . The weighting factors for the dissociation of  $XYZ^*$  into X+YZ and XY+Z were termed partitioning factors  $^{33,34}$  and denoted by  $Y_a$  and  $Y_b$ . The Ys are given later by Eq. (18).

This global transition state for any given quantum state (Jjm) in the full  $\theta$  space  $(0 \text{ to } \pi)$  is determined by the maximum of its energy  $E_{mj}^{J,a}$  along R. The  $E_{mj}^{J,a}$  contains three components: the bond fission energy  $V_0(R)$ , the eigenvalue  $E_{mj}$  of the hindered rotor with quantum number (mj), and the centrifugal-type energy  $(J(J+1)-2m^2)\hbar^2/2\mu R^2$  in Eq. (5). The vibration frequency of the diatomic fragment is taken to be a constant, although such an approximation is readily removed by the use of a sufficiently accurate PES. The diatomic fragment remains in its ground vibrational state due to the large  $O_2$  vibration frequency. Thereby,  $E_{mj}^{J,a}$  also contains the zero-point energy of the oxygen fragment in channel a. The number of states in the transition state for a given (EJ) can then be written as

$$N_{a}(EJ) = \sum_{mj} (2J+1)h(E-E_{mj}^{J,a})\Phi_{a}(mj)$$
 (16)

with  $\Phi_a(mj)$  given by Eq. (15), and  $h(E-E_{mj}^{J,a})$  is a unit step function for  $E-E_{mj}^{J,a}$ . Equations (15) and (16) are next introduced into the appropriate rate expressions.

In the present paper we focus on the isotopic effects for the  $O+O_2+M$  recombination reaction at low third-body (M) pressures, rather than considering all pressures. For existing experiments that is the most important pressure region. In the low-pressure limit the recombination rate constant for the  $X+YZ \rightarrow XYZ$  ( $X \neq Z$ ) is given by the following equation, which was derived earlier<sup>30</sup> using the weak collision model:

$$k_{bi}^{0,a} = \frac{\omega_d - \omega_a}{Q_a} \left( \int_0^{\Delta E} \sum_J \rho(EJ) Y_a(EJ) \right)$$

$$\times e^{-E/k_B T} \frac{\omega}{\omega_d + \omega_a P^o(E)} dE$$

$$+ \int_{\Delta E}^{2\Delta E} \sum_J \rho(EJ) Y_a(EJ)$$

$$\times e^{-E/k_B T} \frac{\omega_d P^c(E - \Delta E)}{\omega_d + \omega_a P^o(E - \Delta E)} dE + \cdots \right), \quad (17)$$

where

$$Y_a(EJ) = \frac{N_a(EJ)}{N_a(EJ) + N_b(EJ)} \tag{18}$$

is the partitioning factor<sup>29,33,34</sup> mentioned earlier. A step-ladder energy transfer model and a strong collisional rotational angular momentum transfer assumption were used in deriving Eq. (17). The  $P^o(E)$  is the fraction of the quantum states in the global transition state that are "open," i.e., whose Js satisfy  $N_a(EJ) + N_b(EJ) > 0$  at the given E. We also have for the "closed" states,  $P^c(E) = 1 - P^o(E)$ . <sup>30</sup>

The quantities appearing in Eqs. (14) and (17) for the rate constants are seen to be the number of states for the hindered rotor, given by Eq. (16), the partition function for the collision pair given by Eqs. (4.8)-(4.12) in Ref. 34, the collision frequencies, and the density of states. The Lennard-Jones collision frequency is used with a unit collision efficiency and is given by Eq. (4.14) of Ref. 34. The density of states for ozone  $\rho(EJ)$  is obtained<sup>34</sup> from a convolution<sup>35,41-43</sup> of the rotational and vibrational density of states at each E and J. The vibration frequencies of the ozone isotopomers used in the calculation were obtained using a second-order perturbation formulation, which gives any unknown frequencies to an accuracy of about 1 cm<sup>-1</sup>.<sup>44</sup> The calculated density of states  $\rho(EJ)$  also includes the anharmonicity, which was obtained<sup>30</sup> using experimental vibrational quantum state energies of <sup>48</sup>O<sub>3</sub>. The anharmonic count for  $\rho(EJ)$  was typically only a factor of 1.5 greater than the

The individual low-pressure rate constants at 300 K for the formation of XYZ molecules were calculated for each channel using Eq. (17). In Tables I–III we give the calculated recombination rate constant ratios for all reactions and com-

TABLE I. Relative rate coefficients of atom plus homonuclear diatomic formation channels  $(X+YY\rightarrow XYY)$  relative to  $X+XX\rightarrow X_3$  at low pressure at 300 K.

Reaction	Expt. <sup>a</sup>	Calc. (present) $\Delta E = 190 \text{ cm}^{-1}$	Calc. (present) $\Delta E = 210 \text{ cm}^{-1}$	Calc. (Ref. 30) $\Delta E = 210 \text{ cm}^{-1}$
$\frac{16O + {}^{36}O_2 / {}^{16}O + {}^{32}O_2}{}$	1.53±0.03	1.53	1.51	1.53
$^{17}O + ^{36}O_2 / ^{17}O + ^{34}O_2$	$1.29 \pm 0.07$	1.34	1.35	1.36
$^{16}O + ^{34}O_2 / ^{16}O + ^{32}O_2$	$1.23 \pm 0.03$	1.36	1.35	1.38
$^{17}O + ^{32}O_2 / ^{17}O + ^{34}O_2$	$1.01 \pm 0.05$	0.99	1.01	1.01
$^{18}O + ^{34}O_2 / ^{18}O + ^{36}O_2$	$1.00 \pm 0.06$	1.06	1.07	1.04
$^{18}O + ^{32}O_2 / ^{18}O + ^{36}O_2$	$0.90 \pm 0.03$	0.90	0.92	0.90

<sup>&</sup>lt;sup>a</sup>From Mauersberger et al., Ref. 25.

TABLE II. Reaction rate coefficients for ozone formation processes relative to  $^{16}O + ^{32}O_2 \rightarrow ^{48}O_3$  at low pressure.

Reaction	Expt.a	Calc. (present) $\Delta E = 190 \text{ cm}^{-1}$	Calc. (present) $\Delta E = 210 \text{ cm}^{-1}$	
$^{16}O + ^{16}O^{16}O$	1.00	1.00	1.00	1.00
$^{17}O + ^{17}O^{17}O$	1.02	1.03	1.02	1.02
$^{18}O + ^{18}O^{18}O$	1.03	1.03	1.03	1.03
$^{18}O + ^{16}O^{16}O$	0.93	0.93	0.95	0.93
$^{17}O + ^{16}O^{16}O$	1.03	1.02	1.04	1.03
$^{18}O + ^{17}O^{17}O$	1.03	1.09	1.10	1.07
$^{17}O + ^{18}O^{18}O$	1.31	1.39	1.38	1.39
$^{16}O + ^{17}O^{17}O$	1.23	1.36	1.35	1.38
$^{16}O + ^{18}O^{18}O$	1.53	1.53	1.51	1.53
$^{16}O + ^{16}O^{17}O^{b}$	1.17	1.18	1.18	1.19
$^{16}O + ^{16}O^{18}O$	1.27	1.25	1.24	1.25
$^{17}O + ^{16}O^{17}O$	1.11	1.03	1.04	1.04
$^{17}O + ^{17}O^{18}O$	1.21	1.22	1.22	1.20
$^{18}O + ^{16}O^{18}O$	1.01	1.00	1.01	0.99
$^{18}O + ^{17}O^{18}O$	1.09	1.06	1.07	1.05
$^{16}O + ^{17}O^{18}O$	_	1.43	1.41	1.43
$^{17}O + ^{16}O^{18}O$	_	1.21	1.21	1.21
$^{18}O + ^{16}O^{17}O$	_	1.01	1.03	1.01

<sup>&</sup>lt;sup>a</sup>From Mauersberger et al., Ref. 25.

pare them there with the experimental values and with the calculated results obtained earlier.<sup>29</sup> The column labeled "Calc. Ref. 30" gives the results obtained before using  $\Delta E = 210 \text{ cm}^{-1}$ . The column "Calc.  $\Delta E = 210 \text{ cm}^{-1}$ " gives present results obtained with the same  $\Delta E$ . The column labeled "Calc.  $\Delta E = 190 \text{ cm}^{-1}$ " gives the present calculation but where the values of  $\eta$  and of  $\Delta E$  were chosen, as in Refs. 29 and 30, to fit two experimental low-pressure recombina-

TABLE IV. Calculated and experimental isotopic enrichments at 300 K.

Reaction	Expt. <sup>a</sup>	Calc. (present) $\Delta E = 190 \text{ cm}^{-1}$	Calc. (present) $\Delta E = 210 \text{ cm}^{-1}$	Calc. (Ref. 30) $\Delta E = 210 \text{ cm}^{-1}$
<sup>16</sup> O <sup>16</sup> O <sup>16</sup> O	0.0	0.0	0.0	0.0
$^{17}O^{17}O^{17}O$	-1.8	-2.1	-1.6	-2.1
$^{18}O^{18}O^{18}O$	-4.6	-4.3	-4.3	-4.7
$^{16}O^{16}O^{17}O^{b}$	11.3	11.5	12.1	12.3
$^{16}O^{16}O^{18}O$	13.0	12.7	12.7	12.7
$^{17}O^{17}O^{16}O$	12.1	11.2	11.2	12.2
$^{17}O^{17}O^{18}O$	9.5	11.7	11.3	10.4
$^{18}O^{18}O^{16}O$	14.4	12.7	12.6	12.7
$^{18}O^{18}O^{17}O$	8.3	9.9	10.3	9.2
<sup>16</sup> O <sup>17</sup> O <sup>18</sup> O	18.1	17.2	17.3	17.4

<sup>&</sup>lt;sup>a</sup>Experimental data at 300 K are from Mauersberger *et al.*, Ref. 25. <sup>b</sup>Enrichments for this and all following rows are for all possible isotopomers.

tion rate constant ratios,  $^{16}\text{O} + ^{18}\text{O}^{18}\text{O} / ^{16}\text{O} + ^{16}\text{O}^{16}\text{O}$  and  $^{18}\text{O} + ^{16}\text{O}^{16}\text{O} / ^{18}\text{O} + ^{18}\text{O}^{18}\text{O}$ . For the present hindered-rotor transition state the value  $\Delta E = 190 \text{ cm}^{-1}$  was obtained. An  $\eta = 1.18$ , obtained both in this fit and that in Ref. 30, is used in all the calculations.

The rate constant ratios given in Tables II and III were then used for the calculation of the enrichments of all possible species of ozone. The latter are given in Table IV together with the experimental and previous calculated results. The calculated results were obtained from individual isotopomeric rate constants using Eqs. (4.18a), (4.18b), and (4.26) of Ref. 33.

The rate constant for the isotopic exchange reaction  $^{16}\mathrm{O} + ^{18}\mathrm{O}^{18}\mathrm{O} \rightarrow ^{18}\mathrm{O} + ^{16}\mathrm{O}^{18}\mathrm{O}$  was calculated using the modified *ab initio* PES. It is independent of any  $\eta$  and  $\Delta E$  approximations, but it does assume a loss of "memory" in the intermediate  $^{16}\mathrm{O}^{18}\mathrm{O}^{18}\mathrm{O}^*$  formed in the reaction. For the partitioning between the formation of  $^{18}\mathrm{O}^{16}\mathrm{O}^{18}\mathrm{O}^*$  and

TABLE III. Reaction rate coefficients for asymmetric and symmetric channels of recombination reactions, relative to <sup>16</sup>O+<sup>16</sup>O<sub>2</sub>→<sup>16</sup>O<sub>3</sub> at low pressure.

Reaction	Expt. <sup>a</sup>	Calc. (present) $\Delta E = 190 \text{ cm}^{-1}$	Calc. (present) $\Delta E = 210 \text{ cm}^{-1}$	Calc. (Ref. 30) $\Delta E = 210 \text{ cm}^{-1}$
Symmetric products				
$^{16}O + ^{17}O^{16}O \rightarrow ^{16}O^{17}O^{16}O$	_	0.51	0.51	0.51
$^{16}O + ^{18}O^{16}O \rightarrow ^{16}O^{18}O^{16}O$	$0.54 \pm 0.01$	0.52	0.52	0.52
$^{17}O + ^{16}O^{17}O \rightarrow ^{17}O^{16}O^{17}O$	_	0.51	0.51	0.51
$^{17}O + ^{18}O^{17}O \rightarrow ^{17}O^{18}O^{17}O$	_	0.52	0.52	0.51
$^{18}\text{O} + ^{16}\text{O}^{18}\text{O} \rightarrow ^{18}\text{O}^{16}\text{O}^{18}\text{O}$	$0.52 \pm 0.01$	0.52	0.52	0.52
$^{18}\text{O} + ^{17}\text{O}^{18}\text{O} \rightarrow ^{18}\text{O}^{17}\text{O}^{18}\text{O}$	_	0.52	0.53	0.52
Asymmetric products <sup>b</sup>				
$^{18}O + ^{17}O^{16}O \rightarrow ^{18}O^{17}O^{16}O$	_	0.48	0.49	0.47
$^{8}O + ^{18}O^{16}O \rightarrow ^{18}O^{18}O^{16}O$	$0.46 \pm 0.03$	0.48	0.49	0.47
$^{17}O + ^{18}O^{16}O \rightarrow ^{17}O^{18}O^{16}O$	_	0.53	0.54	0.52
$^{17}O + ^{17}O^{16}O \rightarrow ^{17}O^{17}O^{16}O$	_	0.52	0.53	0.53
$^{18}O + ^{18}O^{17}O \rightarrow ^{18}O^{18}O^{17}O$	_	0.54	0.54	0.53
$^{18}O + ^{16}O^{17}O \rightarrow ^{18}O^{16}O^{17}O$	_	0.53	0.54	0.53
$^{17}O + ^{16}O^{18}O \rightarrow ^{17}O^{16}O^{18}O$	_	0.69	0.68	0.70
$^{16}O + ^{16}O^{17}O \rightarrow ^{16}O^{16}O^{17}O$	_	0.67	0.67	0.68
$^{17}O + ^{17}O^{18}O \rightarrow ^{17}O^{17}O^{18}O$	_	0.70	0.69	0.70
$^{16}O + ^{18}O^{17}O \rightarrow ^{16}O^{18}O^{17}O$	_	0.69	0.68	0.69
$^{16}O + ^{16}O^{18}O \rightarrow ^{16}O^{16}O^{18}O$	$0.73 \pm 0.02$	0.74	0.73	0.74
$^{16}O + ^{17}O^{18}O \rightarrow ^{16}O^{17}O^{18}O$	_	0.74	0.73	0.74

<sup>&</sup>lt;sup>a</sup>From Janssen et al., Ref. 26.

<sup>&</sup>lt;sup>b</sup>This rate constant and those in the subsequent rows are the sum of both channels,  $X+YZ \rightarrow XYZ$  and  $X+YZ \rightarrow XZY$ . Each of the rate constants was calculated separately, with the non-RRKM correction applied to any symmetric channel.

<sup>&</sup>lt;sup>b</sup>Reactions are ordered in sequence of increasing zero-point energy difference.

TABLE V. Calculated and experimental rate constants.

k	Reaction	T (K)	Expt.	Calc. (Ref. 30)	Calc. (present) <sup>c</sup>
$k_{\rm bi}^{0  \rm a}$	$^{16}O + ^{32}O_2 + N_2 \rightarrow ^{48}O_3 + N_2$	130	4 <sup>b</sup>	5.2	4.8
0.1		300	0.5 <sup>b</sup>	0.76	0.58
	$k_{\mathrm{bi}} \propto T^{-n}$	130-300	n = 2.6	n = 2.3	n = 2.5
$k_{\rm ex}^{\rm d}$	$^{16}\text{O} + ^{18}\text{O}^{18}\text{O} \rightarrow ^{16}\text{O}^{18}\text{O} + ^{18}\text{O}$	130	5.6 <sup>e</sup>	4.3	$2.6^{f}$
		300	$2.9^{e}$	2.7	1.9 <sup>f</sup>
	$k_{\mathrm{ex}} \propto T^{-m}$	130-300	$m = 0.88 \pm 0.26$	m = 0.53	m = 0.36

<sup>&</sup>lt;sup>a</sup>Units are 10<sup>-33</sup> cm<sup>6</sup> s<sup>-1</sup>.

 $^{16}\mathrm{O^{18}O^{18}O^*}$  from  $^{18}\mathrm{O^{+16}O^{18}O}$ , the partitioning factor was calculated using Eq. (15). For comparison this partitioning was also approximated as 1/2. The integrated wave function method yielded for the isotopic exchange reaction  $^{16}\mathrm{O^{+18}O^{18}O} \rightarrow ^{18}\mathrm{O^{+16}O^{18}O}$  a rate constant of 1.94  $\times\,10^{-12}$  cm $^{-3}$  at 300 K and 2.62×10 $^{-12}$  cm $^{-3}$  at 130 K. (These values are rounded off in Table V.) When  $\Phi_a$  and  $\Phi_b$  are assumed, instead, to be 0.5 these values are virtually unchanged:  $1.98\times10^{-12}$  cm $^{-3}$  and  $2.74\times10^{-12}$  cm $^{-3}$ , respectively. (The number of "significant figures" is significant for comparison of these numbers with each other and not for comparison with the experiment.) Results for the isotopic exchange reaction and for the recombination reaction are compared with the experimental and previous theoretical results in Table V.

## **V. DISCUSSION**

A modified *ab initio* PES available in the literature was used in the present RRKM calculations for ozone recombination and isotopic exchange rate constants. The ratios of the recombination rate constants agreed with those in our earlier studies  $^{29,30}$  which employed instead a free-rotor transition state and a hindered-rotor transition state using a model PES. Given the method of choosing the two unknowns  $\Delta E$  and  $\eta$  from two specific recombination rate constant ratios, the results for the numerous rate constant ratios and enrichments are seen to be virtually unchanged from our previous values.

Although the PES used in the present study is very different in detail from the model PES used in the previous study, as seen from the two potential energy profiles (labeled 000) in Fig. 4, the two surfaces give rather similar results for the isotopic exchange reaction  $^{16}\text{O} + ^{18}\text{O}^{18}\text{O} \rightarrow ^{18}\text{O} + ^{16}\text{O}^{18}\text{O}$ : The model PES used in Ref. 30 gives an isotopic exchange rate constant (300 K) about 40% larger than that given by the modified *ab initio* PES. This difference is partly due to the existence of an effective barrier in the present PES at about 2 Å (Fig. 1). It causes the transition state to occur at smaller Rs and thus decreases the value of the calculated rate constant (smaller "cross section") for the recombination collision. If the negative temperature dependence of the rate constant is written as  $T^{-m}$ , the experimental value of m is  $0.88 \pm 0.26$ . The present calculation yielded a smaller value, 0.36, which

is also smaller than the result (0.53) obtained earlier using the model PES.<sup>30</sup> In contrast, the free-rotor transition state is very different from either of the two tight transition states, since it gives<sup>30</sup> a positive temperature dependence of the isotopic exchange rate constant and a rate constant at 300 K more than three times larger than the present result.

The similarity of exchange rate constants obtained using the two very different potential energy surfaces (the model PES used in Ref. 30 and the modified *ab initio* PES used in this study) is not accidental. It occurs because both surfaces were adjusted  $^{30,32}$  to fit the isotopic exchange rate constants. Although the details of the adiabatic curves for each (JKj) state are very different for the two potential energy surfaces, the effective barrier heights are seen in Fig. 4 to be similar. A reflection of this point is that the sums of quantum states  $\sum_J N(E,J)^{45}$  for the transition state are also similar for both potentials (Fig. 5). Also shown in Fig. 5 is the  $\sum_J N(E,J)$  for a loose transition state. As seen in the comparisons in that Figure (and also from the temperature coefficients discussed above) both hindered rotor-transition states are relatively tight.

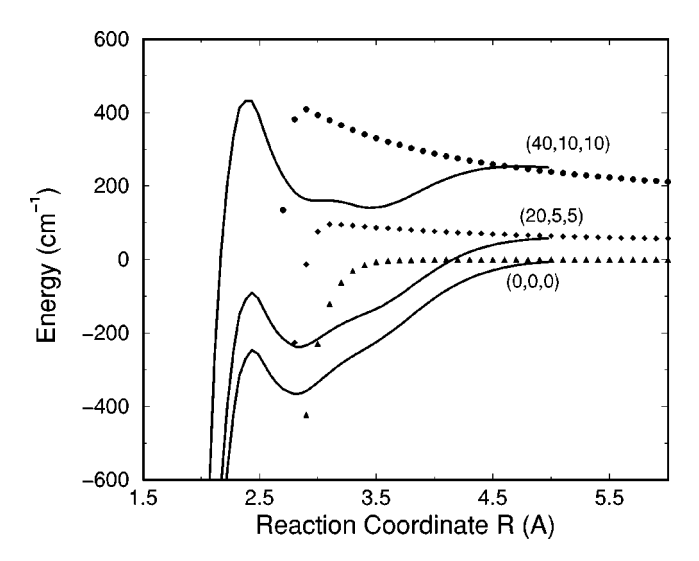


FIG. 4. The energy  $E(Jj\Omega;R)$  of a hindered rotor state  $(Jj\Omega)$  as a function of R for  $^{16}O \cdot \cdot \cdot ^{16}O^{16}O$ . Symbols are obtained using the model potential (Ref. 30) and lines are obtained using the modified *ab initio* PES.

<sup>&</sup>lt;sup>b</sup>Experimental data from Hippler et al., Ref. 37.

<sup>&</sup>lt;sup>c</sup>Calculated using the modified *ab initio* PES and  $\Delta E = 190 \text{ cm}^{-1}$ . When  $\Delta E = 210 \text{ cm}^{-1}$  the values are 5.1 and 0.72, respectively.

<sup>&</sup>lt;sup>d</sup>Units are 10<sup>-12</sup> cm<sup>3</sup> molecule<sup>-1</sup> s<sup>-1</sup>.

<sup>&</sup>lt;sup>e</sup>Experimental data from Wiegell et al., Ref. 31.

<sup>&</sup>lt;sup>f</sup>Calculated using the integrated wave function method.

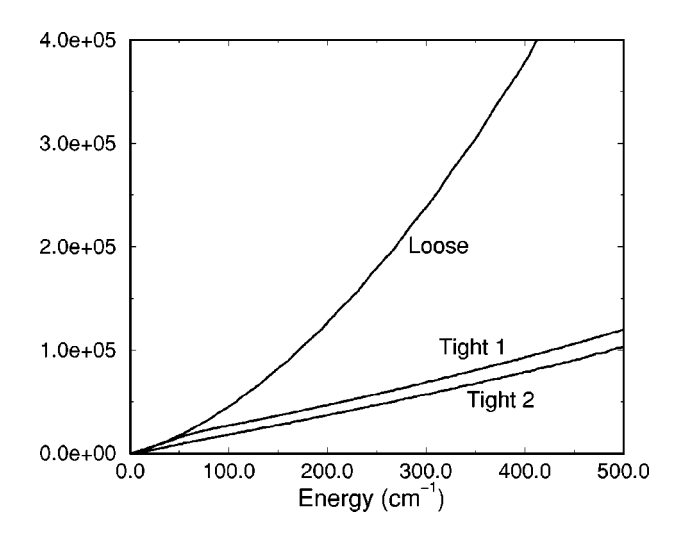


FIG. 5. The number of states  $N_E = \Sigma_J N(EJ)$  as a function of E for the recombination reaction  $^{16}{\rm O} + ^{32}{\rm O}_2 \rightarrow ^{48}{\rm O}_3$ . The curve labeled "Loose" is for a loose transition state, the one labeled "Tight 1" is obtained using the model PES (Ref. 30), and the one labeled "Tight 2" is obtained using the modified *ab initio* PES.

The calculated results for low-pressure recombination rate constants and their ratios are less sensitive to the transition state (and thus to the PES) than the isotopic exchange rate constants. The differences between results obtained using the two tight transition states (this work) and between those obtained using a loose and a tight transition state (Ref. 30) are both small. For example, the model PES gives a low pressure recombination rate constant for \$^{16}O + ^{16}O^{16}O\$  $\rightarrow$  <sup>48</sup>O<sub>3</sub> within 10% of that given by the model PES at both 130 and 300 K when the same  $\Delta E$  is used (footnote c of Table V). The insensitivity of the low-pressure recombination rate constant ratios to the PES is seen clearly in Tables I-III, by comparing the third with the fourth and fifth columns. The third and fifth columns were obtained using a  $\Delta E$ optimized for each PES and the third and fourth columns were obtained using the same  $\Delta E$ , which is optimized for the present surface.

The reasons for the weak dependence of the low pressure recombination results on the PES are several-fold: The dependence of the low pressure recombination rate constants for symmetric molecules on the number of states at the transition state,  $h(N_a(EJ))$ , and that of the recombination rate constant for an asymmetric molecule,  $N_a(EJ)/(N_a(EJ))$  $+N_b(EJ)$ ), are both expected to be weaker than that of the isotopic exchange rate constant. The latter is not only proportional to  $N_a(EJ)/(N_a(EJ) + N_b(EJ))$  but also to  $N_b(EJ)$ , as discussed earlier.<sup>30</sup> In addition, since the  $\Delta E$  per collision was varied to fit two experimental recombination rate constant ratios and then used to calculate all the other ratios, the differences in the rate constant ratios obtained using the two different surfaces are further reduced. For example, to fit the experimental recombination rate constant ratios, values of 260, 210, and 190 cm<sup>-1</sup> were chosen for  $\Delta E$  when the loose transition state and the previous and present tight transition states were used, respectively. Accordingly, the calculated rate constant ratios and thus the enrichments are essentially the same under the three different conditions.

Since a recombination reaction X+YZ ( $Y\neq Z$ ) can lead to two different products, the partitioning between the two products at the same hindered-rotor transition state is of interest. In earlier studies, it was assumed that half of the quantum states of the transition state in the entrance channel lead to one ozone isotopomer XYZ and half to the other, XZY. In the present study, a more general approach is used, where the assignment of the transition quantum state to each product was determined by an integral of its wave function (squared) over half of the  $\theta$  space, the space that leads to that particular molecule as in Eq. (15). As noted in Sec. IV, no significant difference between the two sets of results was found for the isotopic exchange rate constants, or for the recombination rate constants, between the approximate ( $\Phi_a = \Phi_b = 0.5$ ) and the integrated wave function treatment for this partitioning.

It has been pointed out that the large variation in recombination rate constant ratios correlate empirically well with ratios of moment of inertia, 34 differences in zero-point energies, 34,46 and ratios of reduced masses. 34 Indeed, all three quantities are mathematically related to each other 34 and so one cannot determine which of the three factors dominates simply from a plot of the rate constant ratios versus any one of them. 34,47 The theory 29,30 brings out that of the three it is the zero-point energy difference that is the primary source of the large mass-dependent effect in the recombination rate constant ratios, because of its effect on numbers of states in transition states of the two dissociation channels.

#### **ACKNOWLEDGMENT**

It is a pleasure to acknowledge the support of this research by the National Science Foundation.

- <sup>1</sup>R. N. Clayton, L. Grossman, and T. K. Mayeda, Science **182**, 485 (1973).
- <sup>2</sup>J. E. Heidenreich III and M. H. Thiemens, J. Chem. Phys. **78**, 892 (1983).
- <sup>3</sup> J. E. Heidenreich III and M. H. Thiemens, J. Chem. Phys. **84**, 2129 (1986).
- <sup>4</sup>K. Mauersberger, Geophys. Res. Lett. **14**, 80 (1987).
- <sup>5</sup>J. Yang and S. Epstein, Geochim. Cosmochim. Acta **51**, 2011 (1987).
- <sup>6</sup>J. Yang and S. Epstein, Geochim. Cosmochim. Acta **51**, 2019 (1987).
- <sup>7</sup>M. H. Thiemens and T. Jackson, Geophys. Res. Lett. **14**, 624 (1987).
- <sup>8</sup>M. H. Thiemens and T. Jackson, Geophys. Res. Lett. **15**, 639 (1988).
- <sup>9</sup>S. M. Anderson, J. Morton, and K. Mauersberger, Chem. Phys. Lett. **156**, 175 (1989).
- <sup>10</sup>J. Morton, B. Schueler, and K. Mauersberger, Chem. Phys. Lett. **154**, 143 (1989).
- <sup>11</sup>J. Morton, J. Barnes, B. Schueler, and K. Mauersberger, J. Geophys. Res., [Atmos.] **95**, 901 (1990).
- <sup>12</sup>M. H. Thiemens and T. Jackson, Geophys. Res. Lett. 17, 717 (1990).
- <sup>13</sup>B. Schueler, J. Morton, and K. Mauersberger, Geophys. Res. Lett. 17, 1295 (1990).
- <sup>14</sup>J. Wen and M. H. Thiemens, Chem. Phys. Lett. 172, 416 (1990).
- J. Wen and M. H. Thiemens, J. Geophys. Res., [Atmos.] 96, 10911 (1991).
   S. M. Anderson, K. Mauersberger, J. Morton, and B. Schueler, ACS Symp.
- <sup>17</sup>M. H. Thiemens, ACS Symp. Ser. **502**, (1992).
- <sup>18</sup> K. Mauersberger, J. Morton, B. Schueler, J. Stehr, and S. M. Anderson, Geophys. Res. Lett. **20**, 1031 (1993).
- <sup>19</sup>D. Krankowsky, F. Bartecki, G. G. Klees, K. Mauersberger, and K. Schellenbach, Geophys. Res. Lett. 22, 1713 (1995).
- <sup>20</sup> J. Sehested, O. J. Nielsen, H. Egsgaard, N. W. Larsen, T. Pedersen, L. K. Christensen, and M. Wiegell, J. Geophys. Res., [Atoms.] 100, 20979 (1995).
- <sup>21</sup>D. Krankowsky and K. Mauersberger, Science 274, 1324 (1996).

- <sup>22</sup>L. K. Christensen, N. W. Larsen, F. M. Nicolaisen, T. Pedersen, G. O. Sørensen, and H. Egsgaard, J. Mol. Spectrosc. 175, 220 (1996).
- <sup>23</sup> J. C. Johnson and M. H. Thiemens, J. Geophys. Res., [Atmos.] **102**, 25395 (1997).
- <sup>24</sup> S. M. Anderson, D. Hüsebusch, and K. Mauersberger, J. Chem. Phys. **107**, 5385 (1997).
- <sup>25</sup> K. Mauersberger, B. Erbacher, D. Krankowsky, J. Günther, and R. Nickel, Science 283, 370 (1999).
- <sup>26</sup>C. Janssen, J. Günther, D. Krankowsky, and K. Mauersberger, J. Chem. Phys. 111, 7179 (1999).
- <sup>27</sup> J. Guenther, B. Erbacher, D. Krankowsky, and K. Mauersberger, Chem. Phys. Lett. **306**, 209 (1999).
- <sup>28</sup> J. Günther, D. Krankowsky, and K. Mauersberger, Chem. Phys. Lett. 324, 31 (2000).
- <sup>29</sup> Y. Q. Gao and R. A. Marcus, Science **293**, 259 (2001).
- <sup>30</sup> Y. Q. Gao and R. A. Marcus, J. Chem. Phys. **116**, 137 (2002).
- <sup>31</sup> M. R. Wiegell, N. W. Larsen, T. Pedersen, and H. Egsgaard, Int. J. Chem. Kinet. 29, 745 (1997).
- <sup>32</sup> A. Gross and G. D. Billing, Chem. Phys. **217**, 1 (1997).
- <sup>33</sup>B. C. Hathorn and R. A. Marcus, J. Chem. Phys. **111**, 4087 (1999).
- <sup>34</sup>B. C. Hathorn and R. A. Marcus, J. Chem. Phys. 113, 9497 (2000).
- <sup>35</sup>R. G. Gilbert and S. C. Smith, *Theory of Unimolecular and Recombina*tion Reactions (Blackwell Scientific, Boston, 1990), and references cited therein
- <sup>36</sup> K. Yamashita, K. Morokuma, F. Le Quere, and C. Leforestier, Chem. Phys. Lett. **191**, 515 (1992); C. Leforestier, F. Le Quere, K. Yamashita, and K. Morokuma, J. Chem. Phys. **101**, 3806 (1994).
- <sup>37</sup> H. Hippler, R. Rahn, and J. Troe, J. Chem. Phys. **93**, 6560 (1990).
- <sup>38</sup>The neglect of off-diagonal elements  $(\Omega' \neq \Omega)$  in treating the radial motion of the two reactants has been termed in the collision dynamics literature the " $j_z$ -conserving," "coupled state," or "centrifugal decoupling"

- approximation. See for example, R. B. Walker and J. C. Light, Chem. Phys. **7**, 84 (1975).
- <sup>39</sup> Strictly speaking a boundary of the channels leading from X+YZ to XYZ and to XZY does not occur at a  $\theta$  exactly equal to  $\pi/2$  when  $Y \neq Z$ . An improved boundary would be at a  $\theta = \alpha$  where the distance of X to Y equals that from X to Z. The  $\alpha$  depends on R and r via  $\alpha = \cos^{-1}\{(m_Z m_Y)/[2(m_Y + m_Z)]r/R\}$ , where  $m_{Y,Z}$  is the mass of Y (Z). For hindered rotation the typical amplitude tends to be largest in the interior of each  $\theta$  region rather than at  $\theta$  near  $\pi/2$ . We omit the possible refinement of calculating  $\alpha$  instead of using  $\alpha = \pi/2$ . The present treatment permits one to allow for any asymmetry in the wave function between the two  $\theta$  intervals.
- <sup>40</sup> S. Zhang and J. Jin, Computation of Special Functions (Wiley, New York, 1996), Chap. 15.
- <sup>41</sup>T. Baer and W. L. Hase, *Unimolecular Reaction Dynamics, Theory and Experiment* (Oxford University Press, New York, 1996), and references cited therein.
- <sup>42</sup> W. Forst, *Theory of Unimolecular Reactions* (Academic, New York, 1973) and references cited therein.
- <sup>43</sup>P. J. Robinson and K. A. Holbrook, *Unimolecular Reactions* (Wiley-Interscience, London, 1972), and references cited therein.
- <sup>44</sup>B. C. Hathorn and R. A. Marcus, J. Phys. Chem. A **105**, 2612 (2001).
- $^{45}\Sigma_J N(EJ)$  does not appear as such in the rate constant in Ref. 30, but for discussion is a reflection of the tightness or looseness of the transition state.
- <sup>46</sup>C. Janssen, J. Guenther, K. Mauersberger, and D. Krankowsky, Phys. Chem. Chem. Phys. 3, 4718 (2001).
- <sup>47</sup>R. A. Marcus, Science **294**, 951a (2001); www.sciencemag.org/cgi/ content/full/294/5544/951a